

Research

SHORT COMMUNICATION

5% Efficient Evaporated Solid-phase Crystallised Polycrystalline Silicon Thin-film Solar Cells

O. Kunz^{*†}, Z. Ouyang, S. Varlamov and A. G. Aberle[‡]

Photovoltaics Centre of Excellence, The University of New South Wales, Sydney, NSW 2052, Australia

The first energy conversion efficiencies of over 5% are reported for evaporated solid-phase crystallised (SPC) polycrystalline silicon thin-film solar cells. All cells have a size of 2 cm² and are formed on planar glass superstrates. Back surface reflectance is provided by a simple coating with commercial white paint. The best cells have short-circuit current densities of about 19 mA/cm² and external quantum efficiencies peaking at above 80%. The diffusion length in the base of the solar cells is larger than the base thickness, providing significant room for further efficiency improvements via an increased thickness of the base layer. Additional improvements are expected via the use of textured glass sheets, boosting the light trapping capabilities of the cells. Copyright © 2009 John Wiley & Sons, Ltd.

KEY WORDS: thin-film solar cells; energy conversion efficiency; polycrystalline silicon; solid-phase crystallisation; quantum efficiency; diffusion length

Received 10 December 2008; Revised 21 April 2009

Thin-film solar cell technologies receive increasing interest from the photovoltaics (PV) industry¹ due to their potential to produce electricity at significantly lower cost compared to wafer based crystalline Si (c-Si) technologies. This cost reduction is possible through the combination of large-area deposition onto low-cost foreign substrates, more streamlined processing and monolithic cell interconnection, while at the same time consuming only a fraction of the expensive semiconductor material.^{2–4} Polycrystalline silicon (pc-Si or poly-Si) on glass is a promising thin-film PV technology since it makes use of an abundant raw material and since it benefits from decades of expertise that has been gained with c-Si in the semiconductor industry. Compared to other thin-film PV technologies,

such as CdTe, CIGS and a-Si:H/ μ c-Si:H, pc-Si on glass offers the advantage of not relying on transparent conducting oxide (TCO) layers for current collection. Furthermore, unlike the a-Si:H based modules, this technology does not suffer from light-induced degradation via the Staebler–Wronski effect.^{5,6} State-of-the-art solid-phase crystallised (SPC) pc-Si on glass mini-modules have recently surpassed the 10% efficiency mark, with an open-circuit voltage of about 500 mV and a short-circuit current density of nearly 30 mA/cm².^{7,8}

In order to make the pc-Si on glass technology economically competitive in the rapidly growing PV market, it is desirable or even necessary to further increase its efficiency and to reduce the associated module production cost.^{9,10} Presently, crystalline silicon on glass (CSG) solar is the only manufacturer of poly-Si on glass modules. The CSG module production¹¹ is based on a batch deposition of a-Si:H using large-area PECVD (plasma enhanced

* Correspondence to: O. Kunz, Photovoltaics Centre of Excellence, The University of New South Wales, Sydney, NSW 2052, Australia.
†E-mail: o.kunz@unsw.edu.au

‡Present address: Solar Energy Research Institute of Singapore, National University of Singapore, Singapore 117576, Singapore.

chemical vapour deposition) reactors (KAI-1200 from Oerlikon Solar). The PECVD of a-Si has the advantage of being reliable and well proven, since KAI reactors were initially developed for the AM-LCD display industry.¹² The downside is a rather high cost of such PECVD tools and low achievable deposition rates (of the order of 30 nm/min). This is particularly problematic for the production of PV modules where the Si deposition step accounts for a significantly larger fraction of the final product cost compared to LCD displays.¹¹ E-beam evaporation as an emerging alternative deposition method of the a-Si films can potentially lead to substantial cost savings because of a much higher deposition rate (up to 1 $\mu\text{m}/\text{min}$) and the feasibility of continuous in-line processing.^{13,14} High-throughput evaporators are industrially used for barrier coatings and optical coatings. However, their application for the PV industry needs yet to be developed.

In the present paper, we demonstrate that e-beam deposited SPC poly-Si thin-film solar cells are capable of achieving respectable efficiencies in excess of 5% on planar glass superstrates. This result is particularly encouraging since only minor light trapping is present in these devices through a simple pigmented diffuse back surface reflector (BSR)—commercial white paint.¹⁵

Figure 1 presents the good progress that has been made with this solar cell type within the last two years. The best conversion efficiencies of evaporated SPC poly-Si thin-film solar (EVA) cells achieved at UNSW from different developmental stages are displayed. Stage I represents a mesa-type sample that is added for reference purposes.¹⁶ The corresponding sample size is about 0.136 cm^2 and the cell was deposited in substrate configuration. In this case the emitter was contacted with a TCO layer. The stages IIa and IIb are the first

cells produced with the metallisation scheme developed at UNSW. The improvement for the cell of stage III was achieved through the application of a pigmented diffuse BSR. The cell of stage IV had an inverted structure, i.e. an *n*-type base and thicker aluminium fingers. This led to a significant performance increase, particularly due to a decrease in series resistance leading to a higher fill factor (FF). The improvement of the *p*-type EVA cell of stage V is related to a reduced absorber doping and to a further decrease in series resistance. More details on these improvements can be found elsewhere.^{17–19} In the present paper, we concentrate on the last stage (VI) and discuss the corresponding device performance in some detail, as well as the steps that were taken to achieve this promising efficiency result.

The devices are referred to as EVA solar cells, due to the use of *evaporated* a-Si precursor diodes.¹³ The a-Si diodes are deposited by means of e-beam evaporation under non-ultrahigh vacuum conditions (base pressure $\sim 2\text{--}3 \times 10^{-8}$ mbar, deposition pressure $\sim 1\text{--}2 \times 10^{-7}$ mbar) onto planar $5 \times 5 \text{ cm}^2$ SiN-coated borosilicate glass superstrates from Schott AG (Borofloat33). The SiN layer serves as both the antireflection coating and as barrier layer for contaminants from the glass. It can be deposited by PECVD or sputtering.²⁰ The dopants (B and P) are added *in situ* during the a-Si deposition process using high-temperature effusion cells. The presented solar cells are used in the superstrate configuration, i.e. illumination is performed onto the glass side of the devices. The emitter is therefore located directly on the SiN layer, while the back-surface-field (BSF) layer is located at the air-side surface of the devices. After SPC (≥ 24 h at 600°C), the poly-Si diodes receive a rapid thermal anneal (RTA) at a temperature of $\sim 900^\circ\text{C}$ for ~ 4 min to activate dopants and to anneal point defects in the poly-Si films. The diode fabrication process is completed with a defect passivation treatment in a hydrogen plasma at plateau temperatures of $\sim 650^\circ\text{C}$ for ~ 20 min. The plasma termination temperature is 350°C . In this work the hydrogen passivation is achieved using a low-pressure chemical vapour deposition (LPCVD) system with an inductively coupled remote plasma source. The post-deposition treatments RTA and hydrogenation are essential for achieving appreciable efficiencies of SPC poly-Si solar cells on glass, for both silicon deposition technologies (PECVD and evaporation).^{21,22} The total thickness d_{Si} of the poly-Si films is currently around 2 μm , but is likely to increase in the near future as explained below.

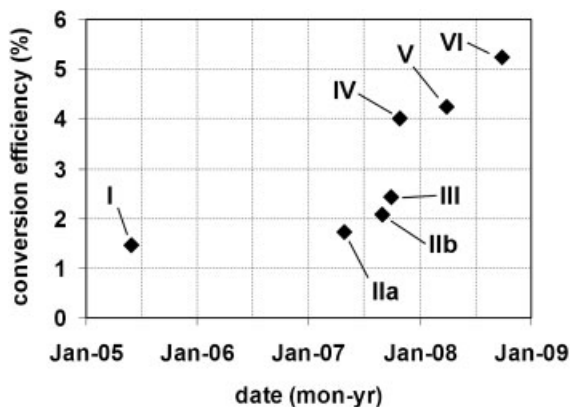


Figure 1. Evolution of EVA cell efficiency at UNSW

All cells of this work were metallised using the device fabrication scheme recently developed at our Centre.¹⁸ This metallisation scheme utilises Al line contacts located in plasma-etched grooves to contact the highly doped emitter layer. The BSF contact is also established via Al line contacts (4 lines per emitter grid line). A shunt mitigation etch is necessary to remove shunting through sub-micron sized pinholes that are inherent to this material, as described elsewhere.¹⁹ Due to the nature of this device fabrication scheme (using interdigitated line contacts), the resulting EVA solar cells can be illuminated from either side (“bifacial” cells). To enhance the response to long-wavelength light and to mechanically protect the metal electrodes, we apply a thick layer of commercial white paint (Dulux) to the back surface of the metallised solar cells.²³ The structure of a metallised EVA solar cell with and without the white paint BSR is schematically displayed in Figure 2, while typical design parameters of *p*-type EVA cells are summarised in Table I.

The main benefit of the white paint BSR is that a large fraction of the photons reaching the rear solar cell surface are returned back into the silicon, thus minimising the fraction of photons that escape at the air side of the cell. The white and grey arrows in Figure 2 represent possible light paths. Weakly absorbed photons returned by the BSR thus travel at least twice through the silicon film. Pathlength enhancement due to oblique light paths (resulting from the scattering events in the pigmented BSR) is also present. However, this effect is rather modest since the refractive index mismatch at the BSR/silicon

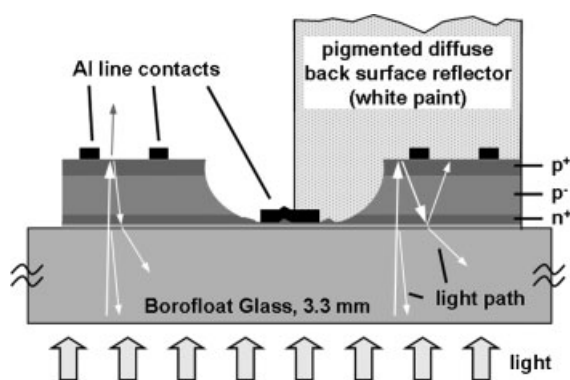


Figure 2. Schematic of an EVA solar cell in the superstrate configuration. To illustrate the different light paths, both BSR cases (air or white paint) are shown in this schematic. (Note that for the results reported in this work—unless stated otherwise—the paint was applied to the entire rear surface of the solar cells.)

Table I. Design parameters of *p*-type EVA solar cells in superstrate configuration

Parameter	Details
Glass	3.3 mm; borosilicate, planar
AR coating	60–70 nm; SiN; PECVD; $n \approx 2.1$
Emitter	~ 200 nm, n^+ ; ~ 400 Ω/sq
Base	~ 1800 nm; p^- ; deposited at ~ 300 nm/min
BSF	~ 100 nm; p^+ ; ~ 1000 Ω/sq
Back reflector	commercial white paint
SPC	≥ 24 h at 600°C
RTA	4 min at $\sim 900^\circ\text{C}$
Hydrogenation	20 min at $\sim 650^\circ\text{C}$; remote plasma

interface tends to refract light toward the interface normal. The resulting light has approximately a “focused Lambertian” distribution with a scattering half angle of only about $24\text{--}33^\circ$ due to the low refractive index of the BSR layer ($n_{\text{BSR}} \approx 1.5\text{--}2$).¹⁵

After metallisation into 2 cm^2 devices, the base doping density N of the cells is measured using impedance analysis (Z-analysis).²⁴ This method determines the *active* base doping density in the absorber layer of the solar cell. We use impedance analysis instead of the classical capacitance analysis because it is more tolerant to diode non-idealities such as a high series resistance R_s , a low shunt resistance R_{sh} and a high diode saturation current. These non-idealities are often encountered when developing new types of solar cells. Excellent agreement between the measured Z-analysis data and the small-signal equivalent-circuit model was obtained for all presented cases, leading to a high degree of confidence in the extracted base doping density values.

Table II lists the base doping densities and other measured parameters of a small selection of finished EVA cells. As can be seen, some of the presented cells have a conversion efficiency exceeding 5%. To our knowledge the efficiency of 5.2% is the highest value published as yet for an evaporated SPC silicon solar cell. An important feature of all these EVA cells is the very lightly doped base layer, with an active doping density of well below $1 \times 10^{16}\text{ cm}^{-3}$.

The highest short-circuit current densities achieved so far are around 15 and 19 mA/cm^2 before (Si/air) and after (Si/paint) application of the white paint BSR, respectively. These values are excellent considering that all cells were deposited on planar glass and therefore feature only modest light trapping. It should be noted that, in order to avoid errors from spectral mismatch of our halogen lamp-based solar simulator, we determined all J_{sc} values by multiplication of the

Table II. Measured parameters of selected EVA solar cells. All cells have an area of 2 cm^2 and feature a white paint back surface reflector. The base doping density was determined via Z-analysis and the silicon thickness via optical fitting of the reflectance data. The short-circuit currents of the unpainted (“Si/air”) and painted (“Si/paint”) cells were determined via integration of the EQE data with the AM1.5G solar spectrum. R_{sh} and $p\text{FF}$ resulted from Suns- V_{oc} measurements. L_{eff} was obtained via PC1D fitting of the devices’ quantum efficiencies, assuming a rear surface recombination velocity S_{back} of $1 \times 10^5\text{ cm/s}$

Cell	N (cm^{-3})	d_{Si} (nm)	V_{oc} (mV)	J_{sc} (Si/air) (mA/cm^2)	J_{sc} (Si/Paint) (mA/cm^2)	$p\text{FF}$ (%)	FF (%)	R_{sh} (Ωcm^2)	R_{s} (Ωcm^2)	Eff. (%)	L_{eff} (μm)
A	$2.1\text{E} + 15$	2070	422	14.94	19.21	73.1	64.5	Infinity	1.99	5.23	>3.5
B	$3.2\text{E} + 15$	2080	426	14.54	18.55	72.8	64.4	Infinity	2.35	5.09	2.50
C	$4.6\text{E} + 15$	2132	435	14.41	18.46	72.8	64.7	1380	2.09	5.20	1.75
D	$5.0\text{E} + 15$	2085	429	13.75	17.57	72.6	61.9	Infinity	3.39	4.67	1.60

measured external quantum efficiency (EQE) curves with the AM1.5G solar spectrum and subsequent integration from 300–1200 nm. For each cell, the light intensity of our solar simulator was then adjusted such that the measured J_{sc} agreed with the J_{sc} calculated from the EQE data. The light beam during the EQE measurement was smaller than the total cell area and was placed in the centre of the cells. To validate this approach we also measured a calibrated Si wafer reference cell with the same set-up. The deviation between the cell’s nominal current and the integrated cell current obtained from the EQE measurement was only 0.3%. Additionally, it should be pointed out that this measurement principle still leads to a significant underestimation of the performance of an equivalent large area solar cell because a large portion of light is diverted outside of the active cell area. For our cell size and cell configuration we measured a current loss of about 9% for the best of our cell, i.e. the quoted J_{sc} values can be seen as rather conservative values.²⁵

Prior to this work, the best reported J_{sc} of EVA cells was $15.6\text{ mA}/\text{cm}^2$.¹⁸ The significant J_{sc} improvements reported in this work result mainly from an optimisation of the base doping density, leading to the use of a rather lightly doped base layer ($N \sim 3 \times 10^{15}\text{ cm}^{-3}$). Note that for such a low base doping density the space charge region width of the p - n junction takes up about one third of the base thickness ($\sim 500\text{ nm}$ for $N = 3 \times 10^{15}\text{ cm}^{-3}$ and a forward-bias voltage of 0.4 V) and hence the dominant transport mechanism for a significant fraction of the photo-generated minority carriers is drift rather than diffusion.

In order to distinguish between metallisation and diode related cell properties, we also list the $p\text{FF}$ that is obtained via Suns- V_{oc} measurements²⁶ in Table II. Suns- V_{oc} is a method that measures the open-circuit voltage of a solar cell as a function of the light

intensity. Suns- V_{oc} curves are essentially identical to dark I - V curves with the exception that no series resistance effects are present and that the light-induced current density is not known. A Suns- V_{oc} curve that is shifted by 1 Sun therefore represents a light I - V curve that could be achieved if no series resistance effects were present. Both the $p\text{FF}$ values and the open-circuit voltages are comparatively low for these cells, hinting at some problem with the silicon deposition process. The $p\text{FF}$ and the V_{oc} of the cells are limited by space charge region recombination occurring in the p - n junction depletion region and/or at grain boundaries. This seems to be different to equivalent cells with light absorber doping that are deposited via PECVD and that have much higher V_{oc} and $p\text{FF}$ values. We are unsure what experimental problem presently limits the $p\text{FF}$ and V_{oc} of our EVA cells, but we believe that it is not of a fundamental nature since EVA cells with V_{oc} values of about 500 mV and with $p\text{FF}$ of around 76% were deposited by us in the past.

Compared to our earlier devices, we were able to reduce the series resistance from $\sim 4\text{ }\Omega\text{cm}^2$ to roughly half of this value, leading to improved fill factors FF. This was mainly achieved by (i) deposition of wider contact fingers and (ii) deposition of higher purity Al films. The latter was realised by altering the deposition process (deposition at lower pressure and faster pump down), giving Al films with lower specific resistance. The better conductance is attributed to a reduced oxygen and nitrogen contamination of the evaporated Al films.²⁷

Quantum efficiency (lines and symbols) and reflectance R curves (dashed and solid line) of the best EVA cell made as yet (cell A) are displayed in Figure 3. The notations “Si/air” and “Si/paint” refer to the cases without and with white paint BSR. It should be mentioned that the front Al electrode (see

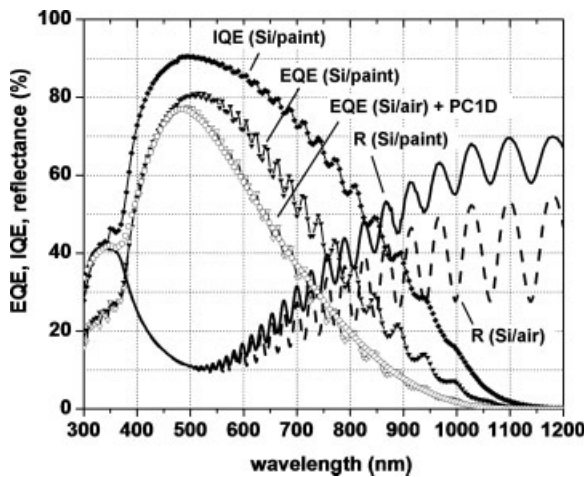


Figure 3. Measured quantum efficiency curves (EQE = triangles; IQE = diamonds) of cell A from Table II prior to (open triangles) and after (filled symbols, “Si/paint”) application of the paint BSR. Note that “Si/air” refers to the case where no paint is present. The reflectance curve of the painted cell (solid line) and the PC1D fit to the EQE curve (no paint) are also shown (open circles)

Figure 2) covers about 3% of the total front surface area of the solar cell, while the rear electrode covers about 15% of the total rear surface. As can be seen, the white paint BSR increases the long-wavelength response considerably, leading to a peak EQE value of about 80% (IQE \sim 90%). The effect of the diffuse BSR on the reflectance curves is seen in increased long-wavelength reflectance values but also in a decrease of the amplitude of the interference fringes. The latter effect is due to diffuse reflection of photons at the Si/paint interface. The reflectance value at the EQE peak wavelength (\sim 500 nm) is about 10%. This is a good value considering the use of planar glass and the fact that \sim 3% of the cell’s front surface is covered by the Al front electrode.

The reflectance and quantum efficiency curves (no paint present) of the cells from Table II were modelled using the one-dimensional numeric device simulator PC1D²⁸ and the standard material parameters for c-Si. Good agreement between the measured and modelled data was achieved in all the cases (see, for example, the open circles in Figure 3). In poly-Si films, the minority carrier transport is affected by recombination processes within the bulk of the grains and at grain boundaries. For this reason a lumped *effective* minority carrier diffusion length L_{eff} needs to be defined in order to describe the minority carrier transport.²⁹ For an efficient solar cell L_{eff} has to be larger than the base

thickness to ensure minority carrier collection from the entire base region. If the base layer is not significantly thinner than L_{eff} , the latter can be determined with good accuracy from the drop of the quantum efficiency curves for $\lambda > \sim$ 500 nm via PC1D fitting. For all cells of this paper the rear surface recombination velocity S_{back} at the Si/air interface was set to 1×10^5 cm/s in the PC1D model. This is a reasonable value for a non-passivated and heavily doped c-Si surface. However, it should be pointed out that the modelled curves are almost completely insensitive to S_{back} . Even when the limiting value of $S_{\text{back}} = 1 \times 10^7$ cm/s was used, L_{eff} was essentially unchanged. No change in the modelled curves could be seen for values of S_{back} lower than 1×10^5 cm/s.

It is evident from Table II that the diffusion length for the two cells with $N < \sim 4 \times 10^{15}$ cm⁻³ is clearly larger than the base layer thickness (which is in the range 1700–1800 nm), allowing the deposition of thicker absorber layers to achieve higher short-circuit currents. An increase in J_{sc} by 1.7 mA/cm² was modelled with PC1D for cell A by changing the modelled base thickness from 1.7–3 μ m and leaving all the other model parameters unchanged. This provides room for further current gains through the deposition of thicker base layers in the case of very lightly doped EVA cells.

Figure 4 presents illuminated J - V data that were measured on cell A. For comparison, and to illustrate the effect of the series resistance, we added the pseudo J - V curve that was obtained from Suns- V_{oc} measurements (solid line). The Suns- V_{oc} data reveal that there is a negligible shunt resistance effect (compare

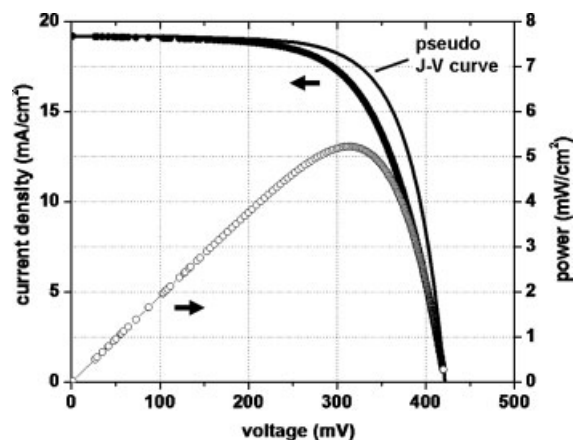


Figure 4. Measured light J - V curve (filled circles) and P - V curve (open circles) of cell A. The corresponding pseudo J - V curve as obtained from Suns- V_{oc} data is also shown (solid line)

Table II) and that the gentle slope of the J - V curve near short-circuit conditions is related to the cell's series resistance. The J_{sc} - V_{oc} data also indicated that there is significant $n = 2$ recombination present in the diode, affecting both the p FF and the open-circuit voltage. The pseudo efficiency $J_{sc} \times V_{oc} \times p$ FF of this device, i.e. the efficiency that would be obtained for $R_s = 0$, is about 5.9%. This demonstrates the necessity to further improve our metallisation scheme to increase the FF (and hence the efficiency) of EVA solar cells. This is particularly important for future devices that are expected to have higher short-circuit current densities due to better light trapping and thicker base layers.

All cells of this work were deposited on planar glass sheets since this simplifies the optimisation of the metallisation scheme and the device structure. However, to increase the light absorption properties of the cells, we have started efforts to transfer the EVA process to textured glass superstrates. The texture is realised with the AIT (aluminium-induced texturisation) method recently developed at UNSW.³⁰ We use mildly textured glass to avoid problems with non-continuous silicon films (film cracking) that can occur as a result of the high directionality of e-beam evaporation as deposition method.³¹ Preliminary results achieved on these mildly AIT textured glass sheets look promising. The silicon films have no cracks and the metallisation can be carried out as usual. Further significant efficiency improvements are thus within reach of the present EVA cell technology.

CONCLUSION

Evaporated SPC poly-Si thin-film solar cells ("EVA" cells) with conversion efficiencies of above 5% were presented. These are the highest efficiencies ever reported for such devices. These efficiencies are respectable if one considers the fact that the cells were formed on planar glass superstrates and they confirm that evaporation is a promising low-cost method for the fabrication of SPC poly-Si thin-film solar cells. Compared to earlier EVA cell results, the improved efficiencies resulted mainly from a lowering of the base doping density, giving significantly higher short-circuit currents. Another important contributor was the reduction of the series resistance via deposition of Al grid fingers with better conductance.

The effective minority carrier diffusion lengths in the base of lightly doped EVA cells have been determined by PC1D modelling of the measured

quantum efficiency. They were found to clearly exceed the base layer thickness of the cells. This provides significant room for efficiency improvements via the deposition of thicker base layers. The open-circuit voltages and pseudo fill factors of the presented solar cells are modest. The reason is not understood but is believed to come from problems during the silicon deposition step and is not inherent to this type of the solar cell. More efficient light trapping is expected to further boost the short-circuit current density and efficiency of EVA solar cells. Thus, the solar cells made from evaporated SPC silicon on foreign substrates appear to be a promising candidate for the low-cost generation of PV electricity.

Acknowledgements

O. Kunz acknowledges a PhD scholarship from the University of New South Wales (UNSW). The Photovoltaics Centre of Excellence at UNSW is one of the Centres of Excellence established and supported by the Australian Research Council (ARC).

REFERENCES

1. Dorn JG. *Solar cell production jumps 50 percent in 2007*, last accessed: December, 2008; available at: <http://www.earthpolicy.org/Indicators/Solar/2007.htm>
2. Aberle AG. Advances in thin film crystalline silicon solar cells. In *Proceedings of the 17th Workshop on Crystalline Silicon Solar Cells and Modules*. Vail: USA, 2007; 71–78.
3. Green MA. Consolidation of thin-film photovoltaic technology: The coming decade of opportunity. *Progress in Photovoltaics: Research and Applications* 2006; **14**: 383–392.
4. Ullal HS, Von Roedern B. 'Thin-film CIGS and CdTe photovoltaic technologies: Commercialization, critical issues and application. In *Proceedings of the 22nd European Photovoltaic Solar Energy Conference*. Milan: Italy, 2007; 1926-L 1929.
5. Chopra KL, Paulson PD, Dutta V. Thin-film solar cells: An overview. *Progress in Photovoltaics: Research and Applications* 2004; **12**: 69–6992.
6. Wronski CR, Von Roedern B, Kolodziej A. Thin-film Si:H-based solar cells. *Vacuum* 2008; **82**: 1145–1150.
7. Green MA, Emery K, Hishikawa Y, Warta W. Solar cell efficiency tables (version 31). *Progress in Photovoltaics: Research and Applications* 2008; **16**: 61–67.
8. Keevers MJ, Young TL, Schubert U, Green MA. 10% efficient CSG minimodules. In *Proceedings of the 22nd European Photovoltaic Solar Energy Conference*. Milan: Italy, 2007; 1783–1790.

9. Swanson RM. A vision for crystalline silicon photovoltaics. *Progress in Photovoltaics: Research and Applications* 2006; **14**: 443–453.
10. Bagnall DM, Boreland M. Photovoltaic technologies. *Energy Policy* 2008; **36**: 4390–4396.
11. Basore PA. CSG-1: Manufacturing a new polycrystalline silicon PV technology. In *Proceedings of the Conference Record of the 2006 IEEE 4th World Conference on Photovoltaic Energy Conversion*. Hawaii 2006; 2089–2093.
12. Shah A, Meier J, Buechel A, Kroll U, Steinhäuser J, Meillaud F, Schade H, Dominé D. Towards very low-cost mass production of thin-film silicon photovoltaic (PV) solar modules on glass. *Thin Solid Films* 2006; **502**: 292–299.
13. Aberle AG, Widenborg PI, Campbell P, Sproul AB, Griffin M, Kunz O, Weber JW, Beilby B, Inns D, Terry ML, Walsh T, He S, Tsao C, Ouyang YZ, Wong J, Hoex B, Shi L, Sakano T, Wolf M, Huang J, Jin G, Huang L, Peng S, Lang M, Schmunk D, Bamberg F, Chan SV, Han J, Ruof T, Berger O, Di D, Fattal A, Gress P, Pelletier M, Mitchell E, Zhou Y, Fecker F, Pohlner S. Poly-Si on glass thin-film PV research at UNSW. In *Proceedings of the 22nd European Photovoltaic Solar Energy Conference*. Milan: Italy, 2007; 1884–1889.
14. Song D, Inns D, Straub A, Terry ML, Campbell P, Aberle AG. Solid phase crystallized polycrystalline thin-films on glass from evaporated silicon for photovoltaic applications. *Thin Solid Films* 2006; **513**: 356–363.
15. Cotter JE, Hall RB, Mauk MG, Barnett AM. Light trapping in silicon-film (TM) solar cells with rear pigmented dielectric reflectors. *Progress in Photovoltaics: Research and Applications* 1999; **7**: 261–274.
16. Song D. Zinc oxide TCOs (transparent conductive oxides) and polycrystalline silicon thin-films for photovoltaic applications, University of New South Wales, Sydney. *PhD Thesis*, June 2005.
17. Kunz O, Ouyang Z, Wong J, Aberle AG. Device fabrication scheme for evaporated SPC poly-Si thin-film solar cells on glass (EVA). In *Proceedings of the IUMRS-ICEM 2008 (international conference on electronic materials)*. Sydney, Australia, 2008; 289–292.
18. Kunz O, Ouyang Z, Wong J, Aberle AG. Advances in evaporated SPC poly-Si thin-film solar cells on glass (EVA). *Advances in OptoElectronics* 2008, 10 pages, Article ID 532351, DOI:10.1155/2008/532351.
19. Kunz O, Wong J, Janssens J, Bauer J, Breitenstein O, Aberle AG. Shunting problems due to sub-micron pinholes in evaporated SPC Poly-Si thin-film solar cells on glass. *Progress in Photovoltaics*, September 2008.
20. Ruske M, Liu J, Wieder S, Preu R, Wolke W. A large area production technology for solar cells—sputter deposition of SiN:H. In *Proceedings of the 20th European Photovoltaic Solar Energy Conference*. Barcelona: Spain, 2005; 1470–1473.
21. Keevers MJ, Turner A, Schubert U, Basore PA, Green MA. Remarkably effective hydrogenation of crystalline silicon on glass modules. In *Proceedings of the 20th European Photovoltaic Solar Energy Conference*. Barcelona: Spain, 2005; 226–229.
22. Terry ML, Inns D, Aberle AG. Rapid thermal annealing and hydrogen passivation of polycrystalline silicon thin-film solar cells on low-temperature glass. *Advances in OptoElectronics* 2007, 11 pages, Article ID 83657, DOI:10.1155/2007/83657.
23. Berger O, Inns D, Aberle AG. Commercial white paint as back surface reflector for thin-film solar cells. *Solar Energy Materials and Solar Cells* 2007; **91**: 1215–1221.
24. Straub A, Gebes R, Habenicht H, Trunk S, Bardos RA, Sproul AB, Aberle AG. Impedance analysis: A powerful method for the determination of the doping concentration and built-in potential of nonideal semiconductor p-n diodes. *Journal of Applied Physics* 2005; **97**: 83703-1–83703-8. DOI: 10.1063/1.1868079.
25. Kunz O. Evaporated Solid-phase Crystallized Poly-silicon Thin-film Solar Cells on Glass, University of New South Wales, Sydney. *PhD Thesis*, 2009.
26. Sinton RA, Cuevas A. A quasi-steady-state open-circuit method for solar cell characterization. In *Proceedings of the 16th European Photovoltaic Solar Energy Conference*. Glasgow: Scotland, 2000; 1152–1155.
27. Hartsough LD, Denison DR. Aluminium and aluminium-alloy sputter deposition for VLSI. *Solid State Technology* 1979; **22**: 66–72.
28. Clugston DA, Basore PA. PC1D version 5: 32-bit solar cell modeling on personal computers. In *Proceedings of the 26th IEEE Photovoltaic Specialists Conference*. Anaheim, USA. 1997; 207–210.
29. Poortmans J, Arkhipov V. *Thin Film Solar Cells: Fabrication, Characterization and Applications*. Chichester, John Wiley & Sons Ltd: 2006.
30. Widenborg PI, Aberle AG. Polycrystalline silicon thin-film solar cells on AIT-textured glass superstrates. *Advances in OptoElectronics*, 2007, September 2007.
31. Ohring M. *The Material Science of Thin Films*. London, Academic Press Limited: 1992.